Formation of prismatic dislocation loops in a spherical particle embedded in a semi-infinite matrix

Jérôme Colin

Version of Record: https://www.sciencedirect.com/science/article/pii/S0020768320302845
Manuscript_8d1b1799e5f8b00115826f8d4ea2055a

Formation of prismatic dislocation loops in a spherical particle embedded in a semi-infinite matrix

Jérôme Colin

Institut Pprime, CNRS-Université de Poitiers, ENSMA, SP2MI-Téléport 2, Futuroscope-Chasseneuil Cedex F86962, France

Abstract

The introduction of prismatic dislocation loops in the interface between a misfitting spherical particle and its semi-infinite matrix has been theoretically investigated. The equilibrium position of one isolated loop has been first determined from an energy variation calculation and a shifting effect on the dislocation position relative to the particle equatorial plane has been identified due to the matrix free-surface. The case of two dislocation loops lying in the particle-matrix interface has been then discussed.

Keywords: Dislocations, Linear Elasticity, Micro-mechanics, Modelling

1. Introduction

The control of the mechanical properties of nanostructured materials is a challenging problem that has been addressed in the last decade in the field of solid mechanics, materials science and metallurgy, because of the numerous applications of such materials in engineering. In case of core-shell nanostructures, the heterogeneity of the lattice parameters (or dilatation coefficients) between the two crystalline phases can produce misfit (thermal) stress that may generate crystalline defects and/or may modify their functional properties. Misfit dislocation loops have been for example identified in GaP-GaN (Lin et al., 2003) and Ge-Si core-shell nanowires (Goldthorpe et al., 2008), and threading dislocations in the core of AlN-GaN coaxial nanowires have been observed to reduce the photoluminescence of the devices (Rigutti et al., 2010). Misfit defects have been also detected in core-shell nanoparticles (CSNPs). For example, high-resolution transmission electron microscopy observations have evidenced perfect misfit dislocations in Fe_3Pt-Fe_2O_3 CSNPs (Liang et al., 2015) and stacking fault, perfect and partial misfit dislocations in Au-Pd CSNPs (Bhattarai et al., 2013). From the theoretical point of view, the formation in core-shell nanowires of different defects such as straight edge dislocations (Gutkin et al., 2000; Raychaudhuri and Yu, 2006), screw dislocations (Wang et al., 2007; Fang et al., 2009; Ahmadzadeh-Bakhshayesh et al., 2012) and dislocation loops (Ovid'ko and Sheinerman, 2004; Aifantis et al., 2007; Raychaudhuri and Yu, 2006; Gutkin et al., 2011) has been investigated and the different critical geometric and physical parameters for the defect nucleation have been identified among which one can cite the different radii of the cores and shells, the elastic coefficients

of the materials and the misfit strains. In CSNPs, the possibility of formation of prismatic dislocation loops and cracks due to misfit stress has been first theoretically investigated by Trusov et al. (1991). The critical conditions for the formation of the circular dislocation loops has been then discussed in details in bulk (Gutkin et al., 2014b; Krauchanka et al., 2019) and hollow (Gutkin et al., 2014a) CNSPs, where it has been found that the equatorial plane is the most favorable one. It is worth noting that the formation of rectangular dislocation loops has been also investigated in CNSPs and the different nucleation sites have been identified (Gutkin and Smirnov, 2014, 2015, 2016). When the axisymmetrical core of a CNSP is truncated, the misfit stress has been computed (Kolesnikova et al., 2018a,b), and the possibility of formation of misfit dislocation loops has been recently analyzed (Gutkin et al., 2020). In particular, it has been found that the optimal sites for the loops are located at a distance of 1/4 of the core radius from the core base.

When a spherical precipitate is embedded in an infinite-size matrix, the critical misfit stress for the nucleation of dislocation loops has been also determined (Jagannadham and Ramachandran, 1974) and, later, the critical radius and critical eigenstrain for a spherical and cylindrical inclusions have been determined and compared (Kolesnikova and Romanov, 2006), the case of cylindrical wires being also examined in details in other works (Fang et al., 2008; Zhao et al., 2012; Shodja et al., 2015). Likewise, the degree of coherency of the interface between a misfitting particle and an infinite-size matrix has been investigated using a three-dimensional level set dislocation dynamics method (Quek et al., 2011). The interaction between the particle and matrix dislocations has been thus studied and the transition from a coherent to semi-coherent interface has been characterized.

In case of a semi-infinite matrix with a planar free-surface, the formation of misfit dislocations in the interfaces of nanowires of rectangular (Gutkin et al., 2003) and cylindrical (Colin, 2016) cross sections has been considered and the effect of the surfaces has been analyzed. Recently, the formation of a dipole of edge dislocations into the interfaces of a misfitting long parallelepipedal nanowire embedded in a thin slab with two horizontal free-surfaces has been investigated. The energy barriers for the dislocation nucleation and the equilibrium positions of the dislocations have been determined (Mikaelyan et al., 2019).

In this framework, the formation of prismatic dislocation loops in the interface between a misfitting spherical inclusion and a semi-infinite matrix has been investigated in this work from an energy variation calculation. Assuming the elastic coefficients are equal in the matrix and the inclusion, the equilibrium positions of one and two loops have been determined and the free-surface effect on the dislocation positions has been characterized.

2. Modeling and Discussion

A spherical particle of radius R is lying in a semi-infinite matrix whose center is located at a distance h from the free-surface (see Fig. 1 for axes). It is assumed in the following that the shear modulus μ and Poisson ratio ν are constant and equal in both phases, with $\nu = 0.3$. Due to the lattice mismatch between the particle and the matrix, an eigenstrain strain $\epsilon^*_{xx} = \epsilon^*_{yy} = \epsilon^*_{zz} = \epsilon_* = 2(a_p - a_m)/(a_p + a_m)$ has been considered into the particle, where a_m and a_p are the lattice parameters of the matrix and the precipitate, respectively

(Mura, 1987). In the following, it is assumed without lack of generality that $a_p > a_m$. The first step of this work has been to determine the resulting misfit strain in the framework of the linear and isotropic theory of elasticity (Timoshenko and Goodier, 1951). The well-known elastic displacement field in the case of a particle embedded in an infinite-size matrix has been first expressed using the spherical coordinate system (r, θ, φ), whose origin O' is the particle center (Teodosiu, 1982; Kolesnikova and Romanov, 2006). Since, for symmetry reason, the elastic field $\mathbf{u}^{i,0} = (u_r^{i,0}, u_\theta^{i,0}, u_\varphi^{i,0})$ is independent of θ and φ variables, it yields:

$$u_r^{p,0}(r) = B_p^0 r, u_\theta^{p,0}(r) = u_\varphi^{p,0}(r) = 0, \tag{1}$$

in the particle $(i = p)$ and

$$u_r^{m,0}(r) = \frac{A_m^0}{r^2}, u_\theta^{m,0}(r) = u_\varphi^{m,0}(r) = 0, \tag{2}$$

in the matrix $(i = m)$. The corresponding elastic strain $\bar{\bar{\epsilon}}^{i,0} = (\epsilon_{kl}^{i,0})$ and stress $\bar{\bar{\sigma}}^{i,0} = (\sigma_{kl}^{i,0})$ tensors have been then expressed using the classical law of the elasticity theory (Timoshenko and Goodier, 1951), with $i = p, m$ and $k, l = r, \theta, \varphi$. The total strain is thus $\epsilon_{kl}^{p,0} + \epsilon_* \delta_{kl}$ in the precipitate and $\epsilon_{kl}^{m,0}$ in the matrix, with δ_{kl} the Kronecker delta. The two constants A_m^0 and B_p^0 have been determined assuming at the interface the total displacement is continuous and the mechanical equilibrium of forces is satisfied (Mura, 1987):

$$\epsilon_* R + u_r^{p,0}(R) = u_r^{m,0}(R), \tag{3}$$

$$\sigma_{rr}^{p,0}(R) = \sigma_{rr}^{m,0}(R). \tag{4}$$

Solving the above system of Eqs., it yields:

$$A_m^0 = \frac{R^3}{3}\frac{1+\nu}{1-\nu}\epsilon_*, \; B_p^0 = -\frac{2}{3}\frac{1-2\nu}{1-\nu}\epsilon_*. \tag{5}$$

When the matrix-free surface is now considered, the correction to the elastic field can be determined taking advantage of the axial symmetry of the composite structure, this problem being already addressed in case of a spherical center of dilatation in a semi-infinite solid (Mindlin and Cheng, 1950). Using now the cylindrical coordinate system (ρ, θ, z) with an origin O located on the matrix free-surface, the previously determined elastic displacement (independent of θ) in the infinite-size matrix has been first rewritten as:

$$u_\rho^{m,0}(\rho, z) = \frac{1+\nu}{1-\nu}\frac{R^3}{3}\epsilon_* \frac{\rho}{(\rho^2 + (z+h)^2)^{3/2}}, u_z^{m,0}(\rho, z) = \frac{1+\nu}{1-\nu}\frac{R^3}{3}\epsilon_* \frac{z+h}{(\rho^2 + (z+h)^2)^{3/2}}, \tag{6}$$

in the matrix and

$$u_\rho^{p,0}(\rho, z) = -\frac{2}{3}\frac{1-2\nu}{1-\nu}\epsilon_* \rho, u_z^{p,0}(\rho, z) = -\frac{2}{3}\frac{1-2\nu}{1-\nu}\epsilon_*(z+h), \tag{7}$$

in the particle. To satisfy the mechanical equilibrium conditions at the free-surface, a relaxation stress $\bar{\bar{\sigma}}_{rel} = (\sigma_{kl}^{rel})$ has been then introduced in the particle and the matrix, in such a way that the mechanical equilibrium of forces is satisfied onto the free-surface:

$$\sigma_{zz}^{m,0}(\rho,0) + \sigma_{zz}^{rel}(\rho,0) = 0, \tag{8}$$
$$\sigma_{\rho z}^{m,0}(\rho,0) + \sigma_{\rho z}^{rel}(\rho,0) = 0. \tag{9}$$

This stress tensor $\bar{\bar{\sigma}}_{rel}$ can be derived from a stress function Ψ_{rel} whose general expression has been expressed using the Hankel transformation as (Sneddon, 1951; Kroupa, 1960):

$$\Psi_{rel}(\rho,z) = \int_0^\infty kG_{rel}(k,z)J_0(k\rho)\,dk, \tag{10}$$

where G_{rel} is a function whose general expression is given by:

$$G_{rel}(k,z) = (A_1 + B_1 z)\exp(kz), \tag{11}$$

with A_1 and B_1 two constants to be determined and J_0 the Bessel function of the first kind and zeroth order. For example, the two components σ_{zz}^{rel} and $\sigma_{\rho z}^{rel}$ present in Eqs. (8) and (9) are given by (Sneddon, 1951; Kroupa, 1960):

$$\sigma_{zz}^{rel}(\rho,z) = \int_0^\infty k\Big[\Big(\frac{2\mu\nu}{1-2\nu}+2\mu\Big)\frac{\partial^3 G_{rel}}{\partial z^3} - \Big(\frac{6\mu\nu}{1-2\nu}+4\mu\Big)k^2\frac{\partial G_{rel}}{\partial z}\Big]J_0(k\rho)dk, \tag{12}$$
$$\sigma_{\rho z}^{rel}(\rho,z) = \int_0^\infty k^2\Big[\frac{2\mu\nu}{1-2\nu}\frac{\partial^2 G_{rel}}{\partial z^2} + \Big(\frac{2\mu\nu}{1-2\nu}+2\mu\Big)k^2 G_{rel}\Big]J_1(k\rho)dk, \tag{13}$$

with J_1 the Bessel function of the first kind and first order. Solving thus the system of Eqs. (8) and (9) with the help of the expressions of the stress components given in Eqs. (12) and (13), the A_1 and B_1 constants have been determined to be:

$$A_1 = (1-2\nu)(1-4\nu)\frac{1+\nu}{1-\nu}\frac{\epsilon_* R^3}{3k^2}e^{-kh}, \tag{14}$$
$$B_1 = (1-2\nu)\frac{1+\nu}{1-\nu}\frac{2\epsilon_* R^3}{3k}e^{-kh}, \tag{15}$$

and the G_{rel} function has been found to be:

$$G_{rel}(k,z) = \frac{(1+\nu)(1-2\nu)}{1-\nu}(1-4\nu+2kz)\frac{\epsilon_* R^3}{3k^2}\exp(k(z-h)). \tag{16}$$

The complete misfit stress is finally defined as $\bar{\bar{\sigma}}_0^{mis,i} = \bar{\bar{\sigma}}_0^i + \bar{\bar{\sigma}}_{rel}$, with $i = p, m$. The problem of the determination of the stress tensor generated by a prismatic dislocation loop of radius r_d, Burgers vector $b\mathbf{e}_z$, whose center is located at $(0,-d)$ in a homogeneous semi-infinite solid has been also addressed, in the framework of the stress function formalism (Kroupa, 1960). This calculation has already been performed in the more general case where the circular prismatic dislocation loop is located near an interface between two heterogeneous

solids (Dundurs and Salamon, 1972). The stress tensor $\bar{\bar{\sigma}}_0^d = (\sigma_{pq}^{d,0})$ of the loop, when it is embedded in an infinite-size matrix at $(0, -d)$, is well-known (Kroupa, 1960; Mura, 1987). For example, the two stress components $\sigma_{\rho z}^{d,0}$ and $\sigma_{zz}^{d,0}$ write in the cylindrical coordinate system (ρ, θ, z):

$$\sigma_{\rho z}^{d,0}(\rho, z, d) = \frac{\mu b \rho_d}{2(1-\nu)} \int_0^\infty (z+d) k^2 J_1(k\rho_d) \exp(-k|z+d|)\, dk, \quad (17)$$

$$\sigma_{zz}^{d,0}(\rho, z, d) = \frac{\mu b \rho_d}{2(1-\nu)} \int_0^\infty k(1+|z+d|) J_1(k\rho_d) \exp(-k|z+d|)\, dk. \quad (18)$$

To satisfy the mechanical equilibrium on the free-surface when the prismatic dislocation loop is now introduced at $(0, -d)$ in the semi-infinite matrix, an image dislocation loop located at $(0, d)$ and of Burgers vector $-b\mathbf{e}_z$ has been first considered (Hirth and Lothe, 1982). Since at the surface ($z = 0$):

$$\sigma_{zz}^{d,0}(\rho, 0, d) - \sigma_{zz}^{d,0}(\rho, 0, -d) = 0, \quad (19)$$

a supplementary stress function ϕ_{sup} generating the stress tensor $\bar{\bar{\sigma}}_{sup} = (\sigma_{kl}^{sup})$ has been thus considered such that:

$$\sigma_{\rho z}^{d,0}(\rho, 0, d) - \sigma_{\rho z}^{d,0}(\rho, 0, -d) + \sigma_{\rho z}^{sup}(\rho, 0) = 0, \quad (20)$$

$$\sigma_{zz}^{sup}(\rho, 0) = 0. \quad (21)$$

The corresponding stress function ϕ_{sup} has been again defined using the Hankel transformation (Sneddon, 1951; Kroupa, 1960):

$$\phi_{sup}(\rho, z) = \int_0^\infty k G_{sup}(k, \rho) J_0(k\rho)\, dk, \quad (22)$$

with:

$$G_{sup}(k, z) = (A_{sup} + B_{sup} z) \exp(kz), \quad (23)$$

and A_{sup} and B_{sup} two constants to be determined. The stress components σ_{zz}^{sup} and $\sigma_{\rho z}^{sup}$ are determined from formulae equivalent to the ones displayed in Eqs.(12) and (13), and from Eqs. (20) and (21), it yields:

$$A_{sup} = -\frac{(1-2\nu)^2}{2(1-\nu)} \frac{b dr_d}{k^2} J_1(kr_d) \exp(-dk), \quad (24)$$

$$B_{sup} = -\frac{(1-2\nu)}{2(1-\nu)} \frac{b dr_d}{k} J_1(kr_d) \exp(-dk). \quad (25)$$

The components of the complete stress tensor generated by the prismatic dislocation loop are finally given by: $\sigma_{kl}^d(\rho, z) = \sigma_{kl}^{d,0}(\rho, z, d) - \sigma_{kl}^{d,0}(\rho, z, -d) + \sigma_{kl}^{sup}(\rho, z)$, with $k, l = \rho, \theta, z$. Once the stress tensors of the misfit and the loop are known, the problem of the dislocation

formation in the particle-matrix interface to release the misfit strain can be addressed from an energy variation calculation. The elastic energy variation of the composite structure ΔE^d_{el} associated with the formation of a loop located at a vertical position $z_d = -d$, from the center of the particle to the interface, can be expressed as (Hirth and Lothe, 1982; Mura, 1987):

$$\Delta E^d_{el} = \pi b \int_0^{\rho_d - a_0} \sigma^d_{zz}(\rho, -d)\, \rho d\rho + 2\pi b \int_0^{\rho_d} \sigma^{mis}_{zz}(\rho, -d)\, \rho d\rho, \tag{26}$$

with a_0 the cut-off radius taken to be equal to b without lack of generality (Hirth and Lothe, 1982). Introducing the functions:

$$I_0(\alpha, \zeta) = \frac{\alpha^{1/2}}{u}\Big[\frac{2-u^2}{2}K(u) - E(u)\Big], \tag{27}$$

$$I_1(\alpha, \zeta) = \frac{\partial}{\partial \zeta} I_0(\alpha, \zeta), \tag{28}$$

$$I_2(\alpha, \zeta) = \frac{\partial^2}{\partial \zeta^2} I_0(\alpha, \zeta), \tag{29}$$

with

$$u^2 = \frac{4\alpha}{(1+\alpha)^2 + \zeta^2}, \tag{30}$$

and K and E the complete elliptic integrals of the first and second kind respectively defined as:

$$K(u) = \int_0^{\frac{\pi}{2}} \frac{d\phi}{(1 - u^2 \sin^2\phi)^{1/2}}, E(u) = \int_0^{\frac{\pi}{2}} (1 - u^2 \sin^2\phi)^{1/2}\, d\phi, \tag{31}$$

the analytic expression of ΔE_{el} has been found to be:

$$\begin{aligned} \Delta E^d_{el} = {} & \frac{\mu b^2}{1-\nu}\rho_d\Big[K\Big(1-\frac{a_0}{\rho_d}\Big) - E\Big(1-\frac{a_0}{\rho_d}\Big) - I_0\Big(1-\frac{a_0}{\rho_d}, \frac{2d}{\rho_d}\Big) + \frac{2d}{\rho_d} I_1\Big(1-\frac{a_0}{\rho_d}, \frac{2d}{\rho_d}\Big) \\ & - \frac{2d^2}{\rho_d^2} I_2\Big(1-\frac{a_0}{\rho_d}, \frac{2d}{\rho_d}\Big)\Big] - \frac{4\pi\mu b \epsilon_*}{3}\frac{1+\nu}{1-\nu}\rho_d^2\Big[1 - R^3 \frac{7d^2 + 8dh + h^2 + \rho_d^2}{(d^2 + 2dh + h^2 + \rho_d^2)^{5/2}}\Big]. \end{aligned} \tag{32}$$

Considering also a core energy ΔE^d_{co} as (Kroupa, 1960):

$$\Delta E^d_{co} = \frac{\mu b^2}{2(1-\nu)}\rho_d, \tag{33}$$

the total energy variation ΔE^d_{tot} due to the formation of the prismatic dislocation loop writes:

$$\Delta E^d_{tot} = \Delta E^d_{el} + \Delta E^d_{co}. \tag{34}$$

Since the loop is lying in the particle-matrix interface, its radius ρ_d can be expressed as $\rho_d = \sqrt{R^2 - (h-d)^2}$, with $h - R < d < h + R$, and the following dimensionless quantities have been introduced, $\tilde{h} = h/b, \tilde{d} = d/b, \tilde{R} = R/b$ and $\Delta\tilde{E}^d_{tot} = \Delta E^d_{tot}/E_0$, with $E_0 = \mu b^3/(1-\nu)$. In Fig. (2), the reduced total energy variation $\Delta\tilde{E}^d_{tot}$ has been plotted versus $\tilde{d}$ for different values of the eigenstrain ϵ_*, with $\tilde{R} = 50$ and $\tilde{h} = 100$. It is observed that as ϵ_* increases, the energy minimum obtained at a particular value of $\tilde{d}$ decreases and becomes negative beyond a critical value $\epsilon^c_* = 0.0093$, this selected distance being thus considered as an equilibrium position $\tilde{d}_{eq}$ for the dislocation loop. To characterize the free-surface effect on this equilibrium position, the quantity $\Delta\tilde{d}_{eq} = \tilde{d}_{eq} - \tilde{h}$ which characterizes the position shift with respect to the equatorial plane of the precipitate has been plotted versus ϵ_* in Fig. (3). When the particle is not to close to the surface ($\tilde{h} = 160$) such that the relaxation of the misfit strain is moderate, the dislocation loop can be attracted by the surface when the eigenstrain is sufficiently low ($\epsilon_* < 0.01$) and $\tilde{d}_{eq} < \tilde{h}$. As the particle gets closer to the surface and the eigenstrain increases, the elastic relaxation in the upper part of the particle increases and the dislocation is repealed inside the lower part of the particle, $\tilde{d}_{eq} > \tilde{h}$, where the misfit strain to be released is more important. It is also underlined that when $\tilde{h} \to \infty$, then $\Delta\tilde{d}_{eq} \to 0$ and the equilibrium position of the dislocation loop tends to the equatorial plane, as expected for a particle embedded in an infinite-size matrix. Finally, the critical radius $\tilde{R}_c$ of the particle beyond which the formation of the prismatic dislocation loop is favorable has been displayed in Fig. (4) versus $\tilde{h}$ for different values of ϵ_*. Discarding the region 3 which is not geometrically acceptable ($\tilde{R}_c > \tilde{h}$), each (blue) curve delimits two other regions. In region 1, the formation of the loop is energetically favorable, while the region 2 corresponds to the configuration where the particle is dislocation-free. The case of the formation of two prismatic dislocation loops of the same Burgers vector $b\mathbf{e}_z$ and located inside the particle at $z_{d_1} = -d_1$ and $z_{d_2} = -d_2$ has been also investigated. The interaction energy $E^{d_1-d_2}_{int}$ between the two loops, whose general expression is given by (Hirth and Lothe, 1982; Mura, 1987):

$$E^{d_1-d_2}_{int} = 2\pi b \int_0^{d_2} \sigma^{d_1}_{zz}(\rho, -d_2)\, \rho d\rho, \tag{35}$$

has been found to be:

$$\begin{aligned} E^{d_1-d_2}_{int} &= \frac{\mu b^2}{1-\nu} 2\rho_{d_1} \Big[I_0\Big(\frac{\rho_{d_2}}{\rho_{d_1}}, \frac{|d_2-d_1|}{\rho_{d_1}}\Big) - I_0\Big(\frac{\rho_{d_2}}{\rho_{d_1}}, \frac{d_2+d_1}{\rho_{d_1}}\Big) - \frac{|d_2-d_1|}{\rho_{d_1}} I_1\Big(\frac{\rho_{d_2}}{\rho_{d_1}}, \frac{|d_2-d_1|}{\rho_{d_1}}\Big) \\ &+ \frac{d_2+d_1}{\rho_{d_1}} I_1\Big(\frac{\rho_{d_2}}{\rho_{d_1}}, \frac{d_2+d_1}{\rho_{d_1}}\Big) - \frac{d_1 d_2}{\rho^2_{d_1}} I_2\Big(\frac{\rho_{d_2}}{\rho_{d_1}}, \frac{d_2+d_1}{\rho_{d_1}}\Big) \Big]. \end{aligned} \tag{36}$$

The total energy variation $\Delta E^{d_1-d_2}_{tot}$ associated with the formation of the two prismatic dislocation loops has been then expressed as:

$$\Delta E^{d_1-d_2}_{tot} = \Delta E^{d_1}_{tot} + \Delta E^{d_2}_{tot} + E^{d_1-d_2}_{int}, \tag{37}$$

where $\Delta E^{d_1}_{tot}$ and $\Delta E^{d_2}_{tot}$ are the energy variations deduced from Eq. (34) resulting from the formation of the dislocations 1 and 2, respectively. Discarding the region $|\tilde{d}_2 - \tilde{d}_1| \leq 1$, the

contourplot of the reduced total energy variation $\Delta E_{tot}^{d_1-d_2}$ has been displayed in Fig. (5) versus $\tilde{d}_1$ and $\tilde{d}_2$, with $\tilde{h} = 100, \tilde{R} = 75$ and $\epsilon_* = 0.02$. It is found that for this level of eigenstrain, there exists two regions in the $(\tilde{d}_1, \tilde{d}_2)$ space, where $\Delta E_{tot}^{d_1-d_2}$ is negative and the formation of the two loops is favorable, these two regions being symmetric with respect to the first diagonal in the $(\tilde{d}_1, \tilde{d}_2)$ plane. The optimal configuration $(\tilde{d}_1^{eq}, \tilde{d}_2^{eq})$ for which the energy variation is minimum has been then determined assuming $\tilde{d}_2^{eq} > \tilde{d}_1^{eq}$ and the dislocation position shifts with respect to the particle center $\Delta\tilde{d}_{eq}^i = \tilde{d}_{eq}^i - \tilde{h}$ have been plotted versus ϵ_* in Fig. (6) for $\tilde{h} = 100$ and $\tilde{R} = 75$, with $i = 1, 2$. It is found that for $\epsilon_* \leq 0.011$, the loops are positioned on both sides of the horizontal plane containing the particle center and when $\epsilon_* > 0.011$, the loops are again located below this plane. As the eigenstrain increases, the two dislocation loops get closer to each other in the lower part of the particle. This position shift of the loops is again attributed to the relaxation effect of the free-surface on the misfit strain, the dislocation being nucleated in the region of higher misfit strain, i.e. in the lower part of the precipitate. Finally, the critical radii $\tilde{R}_c$ of the particle required for the nucleation of one and two dislocation loops have been displayed in Fig. (7) versus ϵ_*, with $\tilde{h} = 100$. In region 1, the formation of the two loops is favorable, in region 2, only one loop can be nucleated and, in region 3, the interface is dislocation-free. It is observed that at constant eigenstrain, the critical radius for the nucleation of two loops is greater than the one required for the formation of only one loop.

3. Conclusion

The formation of one and then two prismatic dislocation loops in the interface between a strained spherical particle and a semi-infinite matrix has been studied from an energy variation calculation. Depending on the misfit strain, it has been found in both cases that the formation of dislocation loops can be energetically favorable. It is also observed that due to the relaxation effect of the free-surface on the misfit strain, the loops are positioned preferentially in the lower part of the particle, when the eigenstrain is sufficiently high. The problem of the nucleation of the loops should be now considered at the microscopic scale using molecular dynamics simulations for example to determine if the dislocations are preferentially nucleated into the particle or at the matrix free-surface. The dislocation pile-up should also be considered in the interface to determine the number (when it is greater than two) and positions of the different dislocations positioned at the interface to release the misfit strain.

References

Ahmadzadeh-Bakhshayesh, H., Gutkin, M.Y., Shodja, H.M., 2012. Surface/interface effects on the elastic behavior of a screw dislocation in an eccentric core-shell nanowire. Int. J. Solids. Struct. 49, 1665–1675. doi:https://doi.org/10.1016/j.ijsolstr.2012.03.020.

Aifantis, K.E., Kolesnikova, A.L., Romanov, A.E., 2007. Nucleation of misfit dislocations and plastic deformation in core/shell nanowires. Philos. Mag. 87, 4731–4757. doi:https://doi.org/10.1080/14786430701589350.

Bhattarai, N., Casillas, G., Ponce, A., Jose-Yacaman, M., 2013. Strain-release mechanisms in bimetallic core–shell nanoparticles as revealed by Cs-corrected STEM. Surf. Sci. 609, 161–166. doi:https://doi.org/10.1016/j.susc.2012.12.001.

Colin, J., 2016. Generation of a dipole of misfit dislocations in an axisymmetrical precipitate embedded in a semi-infinite matrix. Int. J. Sol. Struct. 82, 9–15. doi:https://doi.org/10.1016/j.ijsolstr.2015.12.029.

Dundurs, J., Salamon, N., 1972. Circular prismatic dislocation loop in a two-phase material. Phys. Stat. Sol. (b) 50, 125–133. doi:https://doi.org/10.1002/pssb.2220500115.

Fang, Q.H., Chen, J.H., Wen, P.H., Liu, Y.W., 2009. Misfit dislocations in an annular strained film grown on a cylindrical nanopore surface. Scripta Mater. 60, 395–398. doi:https://doi.org/10.1016/j.scriptamat.2008.11.021.

Fang, Q.H., Liu, Y.W., Chen, J.H., 2008. Misfit dislocation dipoles and critical parameters of buried strained nanoscale inhomogeneity. Appl. Phys. Lett. 92, 121923. doi:https://doi.org/10.1063/1.2903701.

Goldthorpe, I.A., Marshall, A.F., McIntyre, P.C., 2008. Synthesis and strain relaxation of Ge-core/Si-shell nanowire arrays. Nano Lett. 8, 4081–4086. doi:https://doi.org/10.1021/nl802408y.

Gutkin, M., Kuzmin, K.V., Sheinerman, A.G., 2011. Misfit stresses and relaxation mechanisms in a nanowire containing a coaxial cylindrical inclusion of finite height. Phys. Stat. Solidi (b) 248, 1651–1657. doi:https://doi.org/10.1002/pssb.201046452.

Gutkin, M.Y., Kolesnikova, A.L., Krasnitckii, S.A., Romanov, A.E., G., S.A., 2014a. Misfit dislocation loops in hollow core-shell nanoparticles. Scripta Mater. 83, 1–4. doi:https://doi.org/10.1016/j.scriptamat.2014.03.005.

Gutkin, M.Y., Kolesnikova, A.L., Krasnitsky, S.A., Romanov, A.E., 2014b. Misfit dislocation loops in composite core-shell nanoparticles. Phys. Solid State 56, 723–730. doi:https://doi.org/10.1134/S1063783414040106.

Gutkin, M.Y., Kolesnikova, A.L., Mikheev, D.S., Romanov, A.E., 2020. Misfit stresses and their relaxation by misfit dislocation loops in core-shell nanoparticles with truncated spherical cores. Eur. J. Mech. / A Solids 81, 103967. doi:https://doi.org/10.1016/j.euromechsol.2020.103967.

Gutkin, M.Y., Ovid'ko, I.A., Sheinerman, A.G., 2000. Misfit dislocations in wire composite solids. J. Phys. Condens. Matter. 12, 5391–5401. doi:https://doi.org/10.1088/0953-8984/12/25/304.

Gutkin, M.Y., Ovidko, I.A., Sheinerman, A.G., 2003. Misfit dislocations in composites with nanowires. J. Phys.: Condens. Matter 15, 3539–3554. doi:https://doi.org/10.1088/0953-8984/15/21/304.

Gutkin, M.Y., Smirnov, A.M., 2014. Generation of rectangular prismatic dislocation loops in shells and cores of composite nanoparticles. Phys. Sol. Stat. 56, 731–738. doi:https://doi.org/10.1134/S1063783414040118.

Gutkin, M.Y., Smirnov, A.M., 2015. Initial stages of misfit stress relaxation in composite nanostructures through generation of rectangular prismatic dislocation loops. Acta Mater. 88, 91–101. doi:https://doi.org/10.1016/j.actamat.2015.01.020.

Gutkin, M.Y., Smirnov, A.M., 2016. Initial stages of misfit stress relaxation through the formation of prismatic dislocation loops in GaN–Ga_2O_3 composite nanostructures. Phys. Sol. Stat. 58, 1611–1621. doi:https://doi.org/10.1134/S1063783416080138.

Hirth, J., Lothe, J., 1982. Theory of dislocations. John Wiley & Sons, Wiley Interscience Publication.

Jagannadham, K., Ramachandran, E., 1974. Critical misfit for generation of dislocations at second-phase particles. J. Appl. Phys. 45, 2406. doi:https://doi.org/10.1063/1.1663606.

Kolesnikova, A.L., Gutkin, M.Y., Krasnitckii, S.A., Smirnov, A.M., Dorogov, M.V., Serebryakova, V.S., Romanov, A.E., Aifantis, E.C., 2018a. On the elastic description of a spherical janus particle. Rev. Adv. Mat. Sci. 57, 246–256. doi:https://doi.org/10.1515/rams-2018-0070.

Kolesnikova, A.L., Gutkin, M.Y., Romanov, A.E., 2018b. Analytical elastic models of finite cylindrical and truncated spherical inclusions. Int. J. Sol. Struct. 143, 59–72. doi:https://doi.org/10.1016/j.ijsolstr.2018.02.032.

Kolesnikova, A.L., Romanov, A.E., 2006. Misfit dislocation loops and critical parameters of quantum dots and wires. Phil. Mag. Lett. 84, 501–506. doi:https://doi.org/10.1080/09500830412331305274.

Krauchanka, M.Y., Krasnitckii, S.A., Gutkin, M.Y., Kolesnikova, A.L., Romanov, A.E., 2019. Circular loops of misfit dislocations in decahedral core-shell nanoparticles. Scripta Mater. 167, 81–85.

doi:https://doi.org/10.1016/j.scriptamat.2019.03.031.
Kroupa, F., 1960. Circular edge dislocation loop. Chech. J. Phys. 10, 284–293. doi:https://doi.org/10.1007/BF02033533.
Liang, W.I., Zhang, X., Zan, Y., Pan, M., Czarnik, G., Bustillo, K., Xu, J., Chu, Y.H., Zheng, H., 2015. In situ study of Fe_3Pt-Fe_2O_3 core-shell nanoparticle formation. J. Am. Chem. Soc. 137, 14850–14853. doi:10.1021/jacs.5b10076.
Lin, H.M., Chen, Y.L., Yang, J., Liu, Y.C., Yin, K.M., Kai, J.J., Chen, F.R., Chen, L.C., Chen, Y.F., Chen, C.C., 2003. Synthesis and characterization of core–shell GaP@GaN and GaN@GaP nanowires. Nano Lett. 3, 537–541. doi:https://doi.org/10.1021/nl0340125.
Mikaelyan, K.N., Gutkin, M.Y., Borodin, E.N., Romanov, A.E., 2019. Dislocation emission from the edge of a misfitting nanowire embedded in a free-standing nanolayer. Int. J. Solids Struct. 161, 127–135. doi:https://doi.org/10.1016/j.ijsolstr.2018.11.014.
Mindlin, R., Cheng, D., 1950. Thermoelastic stress in the semi-infinite solid. J. Appl. Phys. 21, 931. doi:https://doi.org/10.1063/1.1699786.
Mura, T., 1987. Micromechanics of Defects in Solids. Martinus Nijhoff Publishers, Dordrecht, The Netherlands.
Ovid'ko, I.A., Sheinerman, A.G.K., 2004. Misfit dislocation loops in composite nanowires. Philos. Mag. 84, 2103–2118. doi:https://doi.org/10.1080/14786430410001678163.
Quek, S.S., Xiang, Y., Srolovitz, D.J., 2011. Loss of interface coherency around a misfitting spherical inclusion. Acta Mater. 59, 5398–5410. doi:https://doi.org/10.1016/j.actamat.2011.05.012.
Raychaudhuri, S., Yu, E.T., 2006. Critical dimensions in coherently strained coaxial nanowire heterostructures. J. Appl. Phys. 99, 114308. doi:https://doi.org/10.1063/1.2202697.
Rigutti, L., Fortuna, F., Tchernycheva, M., Bugallo, A.D.L., Jacopin, G., Julien, F.H., Chou, S.T., Lin, Y.T., Tu, L.W., Harmand, J.C., 2010. Optical properties of GaN and GaN/AlN nanowires: the effect of doping and structural defects. Phys. Status Solidi C 7, 2233–2235. doi:https://doi.org/10.1002/pssc.200983472.
Shodja, H.M., Enzevaee, C., Gutkin, M.Y., 2015. Interface effect on the formation of a dipole of screw misfit dislocations in an embedded nanowire with uniform shear eigenstrain field. Eur. J. Mech. A/ Solids 51, 154–159. doi:https://doi.org/10.1016/j.euromechsol.2014.12.006.
Sneddon, J., 1951. Fourier Transforms. McGraw-Hill, New York.
Teodosiu, C., 1982. Elastic Models of Crystal defects. Springer, Verlag Berlin Heidelberg.
Timoshenko, S., Goodier, J., 1951. Theory of Elasticity. McGraw-Hill Book Company Inc, New York.
Trusov, L.I., Tanakov, M.Y., Gryaznov, V.G., Kaprelov, A.M., Romanov, A.E., 1991. Relaxation of elastic stresses in overlayed microcrystals. J. Cryst. Growth 114, 133–140. doi:https://doi.org/10.1016/0022-0248(91)90688-2.
Wang, X., Pan, E., Roy, A.K., 2007. New phenomena concerning a screw dislocation interacting with two imperfect interfaces. J. Mech. Phys. 55, 2717–2734. doi:https://doi.org/10.1016/j.jmps.2007.03.017.
Zhao, Y.X., Fang, Q.H., Liu, Y.W., 2012. Edge misfit dislocation formation at the interface of a nanopore and infinite substrate with surface/interface effects. Phil. Mag. 92, 4230–4249. doi:https://doi.org/10.1080/14786435.2012.705038.

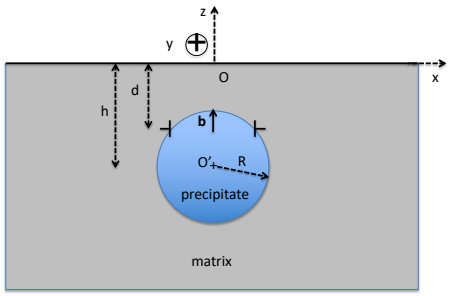

Figure 1: Schematic in the (Oxz) plane of a spherical particle of radius R embedded in a semi-infinite matrix at a distance h from the free-surface. A prismatic dislocation loop of Burgers vector $b\mathbf{u}_z$ is lying in the interface at a distance d from the free-surface.

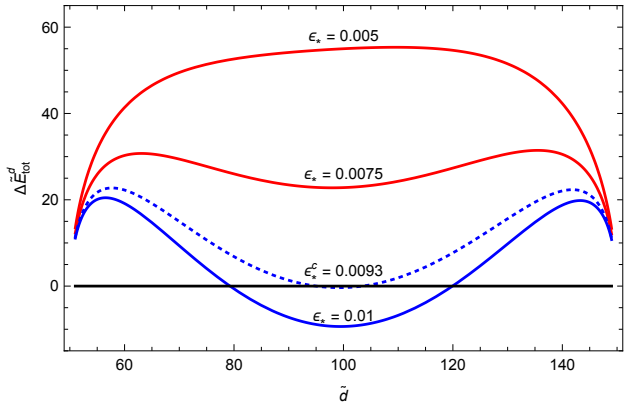

Figure 2: Reduced total energy variation $\Delta\tilde{E}^d_{tot}$ versus $\tilde{d}$ for different values of ϵ_*, with $\tilde{R} = 50$, and $\tilde{h} = 100$.

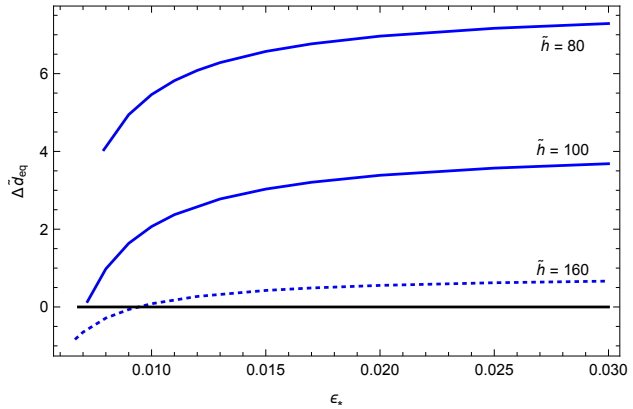

Figure 3: Dislocation position shifts with respect to the particle center $\Delta\tilde{d}_{eq} = \tilde{d}_{eq} - \tilde{h}$ versus ϵ_* for different values of $\tilde{h}$, with $\tilde{R} = 75$.

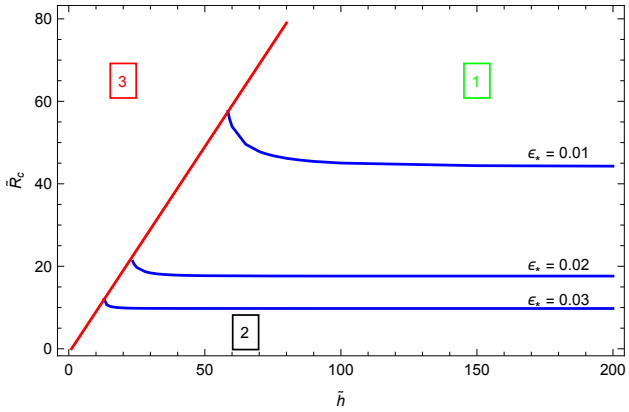

Figure 4: Critical radius $\tilde{R}_c$ of the particle for the nucleation of one dislocation loop versus ϵ_* for different values of $\tilde{h}$. Each blue curve delimits two regions. In region 1, the formation of the loop is favorable, in region 2, the interface is dislocation-free. The region 3 is not geometrically acceptable since $\tilde{R}_c > \tilde{h}$.

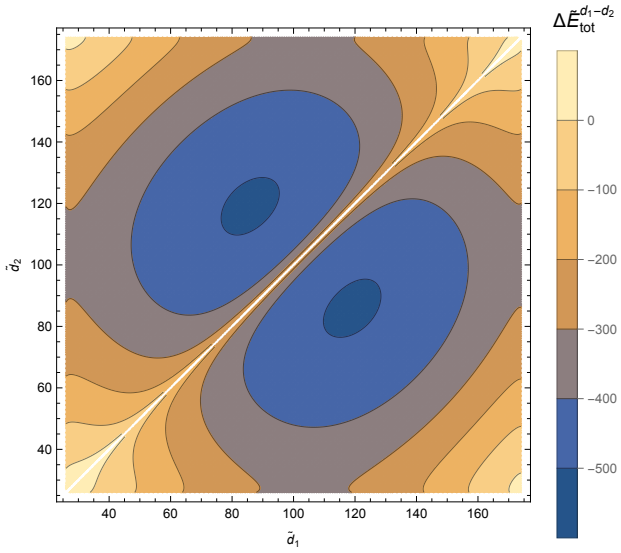

Figure 5: Contourplot of the reduced total energy variation $\Delta E_{tot}^{d_1-d_2}$ versus $\tilde{d}_1$ and $\tilde{d}_2$, with $\tilde{h} = 100, \tilde{R} = 75$ and $\epsilon_* = 0.02$.

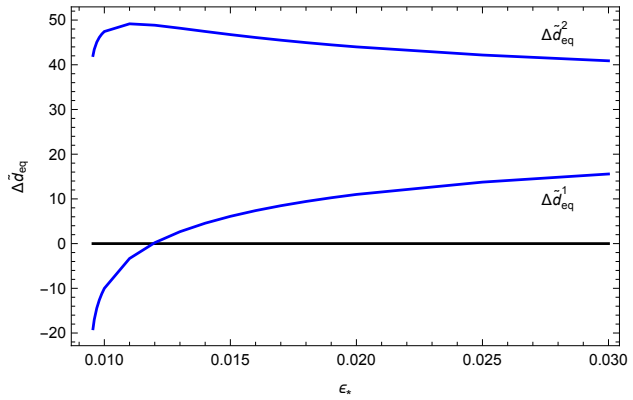

Figure 6: Dislocation position shifts with respect to the particle center $\Delta\tilde{d}^i_{eq} = \tilde{d}^i_{eq} - \tilde{h}$ versus ϵ_* for $\tilde{h} = 100$ and $\tilde{R} = 75$, with $i = 1, 2$.

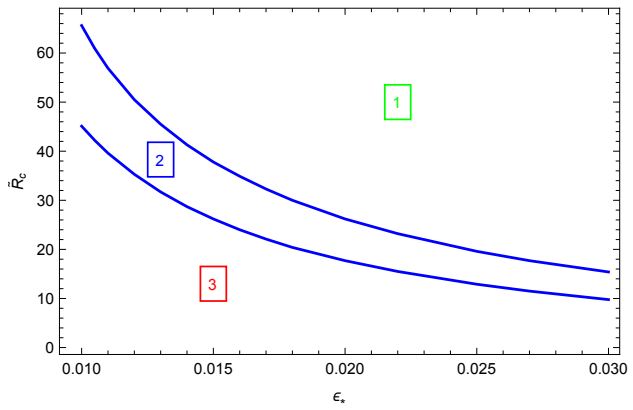

Figure 7: Critical radii $\tilde{R}_c$ of the particle for the nucleation of one and two dislocation loops versus ϵ_*, with $\tilde{h} = 100$. In region 1, the formation of the two loops is favorable, in region 2, only one loop can be nucleated. In region 3, the interface is dislocation free.